THE SOFT WALL MODEL OF THE CASIMIR EFFECT

An Undergraduate Research Scholars Thesis

by

COLIN WHISLER and STEVEN MURRAY

Submitted to Honors and Undergraduate Research
Texas A&M University
in partial fulfillment of the requirements for the designation as

UNDERGRADUATE RESEARCH SCHOLAR

Approved by
Research Advisor: Dr. Stephen Fulling

May 2015

Major: Physics

TABLE OF CONTENTS

Page

ABSTRACT 1

ACKNOWLEDGMENTS 2

I INTRODUCTION 3

II THE SOFT WALL MODEL 7

The Field Equation 7

Stress-Energy Tensor 13

III OUTSIDE THE WALL 17

IV INSIDE THE WALL 22

V CONCLUSIONS 28

REFERENCES 29

ABSTRACT

The Soft Wall Model of the Casimir Effect. (May 2015)

COLIN WHISLER and STEVEN MURRAY
Department of Physics
Texas A&M University

Research Advisor: Dr. Stephen Fulling
Department of Mathematics

In this paper, we examine the Casimir interaction between a scalar field and a boundary analogous to a conducting wall with some small but finite skin depth to electromagnetic radiation with the goal of calculating the energy density and pressure. We model the wall as a soft wall where the potential is given by a monomial function of arbitrary degree. The soft-wall approximation is a useful model because it eliminates some of the divergent terms that arise during the traditional approach to the subject. For the region outside the wall, we show that the principle of virtual work holds, not just formally for the infinite energy, but regardless of the regularization method used to obtain finite interaction energies and pressures. Furthermore, we lay the groundwork to prove this property inside the wall. We present improvements and extensions of prior work in the field by adjusting the approximations used to increase accuracy as well as calculating the pressure. The solution can be applied to the hard-wall case by adjusting the parameters, allowing us to calculate the desired quantities without having to contend with divergences.

ACKNOWLEDGMENTS

We would like to acknowledge Dr. Fulling for his assistance and guidance throughout this project. Our research would not have been possible without his devotion and expertise. We would also like to thank Hamilton Carter and Jeffrey Wagner for helping us move forward with our developments in the soft-wall model. Finally, we would like to acknowledge Kimball Milton and F. D. Mera for reviewing our progress and helping us improve our thesis.

CHAPTER I

INTRODUCTION

The Casimir effect is a phenomenon arising from the interaction between a boundary surface and the vacuum energy from quantum fields [1]. When the field is confined to a finite volume of space, the restrictions on the modes available to the field create a measurable force on the boundary surfaces [2]. The subject has been studied extensively, usually considering flat conducting plates [3]. In this arrangement, the plates can be shown to attract one another with a force inversely proportional to the fourth power of the separation distance. Other developments in the field have been made by examining wedges [4] [5] [6] and spheres [7] [8]. We wish to find the local energy density and pressure, from which all physically interesting quantities may be derived, in a system containing a single boundary surface. There is a standard solution method for Casimir-effect problems, based on a Green's function of the field equation corresponding to the geometry of the system considered. We use this Green's function to find the components of the stress-energy tensor.

The standard approach to the problem is known as the hard wall method. This method uses a Dirichlet boundary condition for a scalar field to create an analogous physical configuration to a perfect conductor in an electromagnetic field in the limit where the skin depth of the conductor goes to zero, thus confining the field to be exactly zero everywhere inside the conductors. However, when the solution is calculated in this way, divergent terms are encountered [9]. The scalar field equation for this configuration is $\frac{\partial^2\Phi}{\partial t^2} = \nabla^2\Phi$ subject to the Dirichlet boundary condition where $\Phi = 0$. The normal modes of the system are $\Phi_n = \frac{1}{\sqrt{2\omega_n}}\phi_n(\boldsymbol{r})e^{-i\omega_n t}$. Each mode acts as a harmonic oscillator with energy $\frac{1}{2}\omega$. When the energy is added over all modes of the system, the total energy becomes $\langle E\rangle = \frac{1}{2}\sum_n \omega_n$. This sum over all modes of the system is clearly divergent. Terms such as these present difficulties to researchers because they do not correspond to physical realities measured in the laboratory. The problem is often resolved using an ultraviolet cutoff to make the integrals over frequency finite (justified by the fact that real materials do not respond to all frequencies of radiation). With this technique, we can write the energy as $\frac{1}{2}\sum_n \omega_n e^{-\omega_n t}$,

where t is an ultraviolet cutoff parameter which can also be considered as a Wick rotation of the difference of two time coordinates, $\tau = -i(t - t')$ [10]. However, this form of regularization gives results for energy density and pressure that are inconsistent with each other. In particular, the so-called principle of virtual work can be disrupted by the regularization method used to obtain finite energy densities and pressures. This principle requires that any change in the vacuum energy due to some infinitesimal movement of a boundary of the system be attributable to some vacuum pressure pushing against that boundary. As an example, consider the pressure against a flat wall,

$$-\frac{\partial E}{\partial x} = F = \iint p dy dz. \tag{I.1}$$

These relations do not follow by default from the local energy-momentum conservation law, $\frac{\partial T^{\mu\nu}}{\partial x^{\mu}} = 0$. They instead constrain the equation of state of the quantized field [6]. For the case of two parallel plates, it can be shown that this pressure relation is indeed satisfied under zeta-function regularization [11]. For more complicated arrangements, such as the wedges and spheres listed above [8] [6], this relation cannot yet be shown to be true for any choice of the regularization method used to remove the divergent free space vacuum energy. Some of these issues can be resolved by performing the point-splitting in a neutral direction; that is, a direction parallel to the wall [10] [12].We aim to bypass these problems by creating a new model that computes the desired quantities in a more physically rigorous framework.

The boundary condition for a hard wall at $z = 1$ is given by the potential

$$V(z) = \begin{cases} 0 & \text{if } z < 1 \\ \infty & \text{if } z > 1 \end{cases} \tag{I.2}$$

The soft-wall model, proposed by Bouas et al. [13] and further studied by Milton [14] and Fulling et al. [12], replaces the Dirichlet boundary condition with a smooth, steeply rising potential function given by

$$V(z) = \begin{cases} 0 & \text{if } z \leq 0 \\ z^\alpha & \text{if } z > 0 \end{cases} \tag{I.3}$$

This potential applies to a soft wall set in the xy-plane, modeling a conducting plate whose thickness is much greater than its skin depth, and whose size is large enough that edge effects are negligible. As the degree of the monomial z^α is raised to infinity, the shape of the potential approaches that of the hard-wall case. Using this potential, we derive the formulas for the Green's function and the stress-energy tensor for the soft wall model of the Casimir effect on a scalar field model of a single conducting plate. We then show that the virtual-work property, as defined above, follows easily from the form of the stress-energy tensor in the region with no potential. We attribute this success to the fact that the soft-wall model is a consistent physical system whose energy density is finite from the start, rather than being forced to be finite by an ad hoc cutoff.

To find the Green's function, we begin with the scalar field function,

$$\frac{\partial^2 \Phi}{\partial t^2} = \nabla^2 \Phi - V(z)\Phi, \tag{I.4}$$

which can be rewritten using a Wick rotation.

$$\frac{\partial^2 \Phi}{\partial \tau^2} + \nabla^2 \Phi - V(z)\Phi = 0 \tag{I.5}$$

This equation can be separated into z and transverse components. The transverse components of the field equation are trivial to solve: the eigenfunctions, which depend on $\sqrt{\zeta^2 + |\boldsymbol{k}_\perp^2|}$, are complex exponentials with constant eigenvalue.

$$\Phi(\boldsymbol{r}, \tau) = \frac{1}{2\pi} e^{i\zeta\tau} e^{i\boldsymbol{k}_\perp \cdot \boldsymbol{r}_\perp} \phi(z) \tag{I.6}$$

Let $\kappa = \sqrt{\zeta^2 + |\boldsymbol{k}_\perp^2|}$ be the magnitude of the combined transverse eigenvalues. The mode function $\phi(z)$, and by extension the reduced Green's function, are determined by the separated field equation

$$\left(-\frac{\partial^2}{\partial z^2} + V(z) + \kappa^2 \right) \phi_\kappa(z) = 0 \tag{I.7}$$

$$\left(-\frac{\partial^2}{\partial z^2} + V(z) + \kappa^2 \right) g_\kappa(z, z') = \delta(z - z'). \tag{I.8}$$

CHAPTER II

THE SOFT WALL MODEL

The Field Equation

Let us begin with the separated field equation and the Green's function equation in natural units:

$$\left(-\frac{\partial^2}{\partial z^2} + V(z) + \kappa^2 \right) \phi_\kappa(z) = 0 \tag{II.1}$$

$$\left(-\frac{\partial^2}{\partial z^2} + V(z) + \kappa^2 \right) g_\kappa(z, z') = \delta(z - z'), \tag{II.2}$$

where $\phi(z)$ is some combination of the two linearly independent solutions to the differential equation, and $g(z, z')$ is the Green's function. Here $\kappa = \sqrt{\zeta^2 + |\boldsymbol{k}_\perp^2|}$ refers to a spectral parameter to be used in the calculation of energy density [14]. Let us consider the first of the two equations. Because this equation is second-order, it will have two linearly independent solutions. We will call these two solutions $F(z)$ and $G(z)$. The normalization conditions used to obtain particular solutions are

$$F(0) = 1 \qquad \lim_{z\to\infty} F(z) = 0 \tag{II.3}$$

$$G(0) = 0 \qquad G'(0) = 1. \tag{II.4}$$

The case $\alpha = 1$ is easily solved using Airy functions, and the case $\alpha = 2$ also produces an exact solution involving parabolic cylinder functions. For $\alpha = 1$, the solutions are

$$F(z) = \frac{\mathrm{Ai}(\kappa^2 + z)}{\mathrm{Ai}(\kappa^2)} \tag{II.5}$$

$$G(z) = \frac{\mathrm{Bi}(\kappa^2)\,\mathrm{Ai}(\kappa^2 + z) - \mathrm{Ai}(\kappa^2)\,\mathrm{Bi}(\kappa^2 + z)}{\mathrm{Ai}'(\kappa^2)\,\mathrm{Bi}(\kappa^2) - \mathrm{Ai}(\kappa^2)\,\mathrm{Bi}'(\kappa^2)}. \tag{II.6}$$

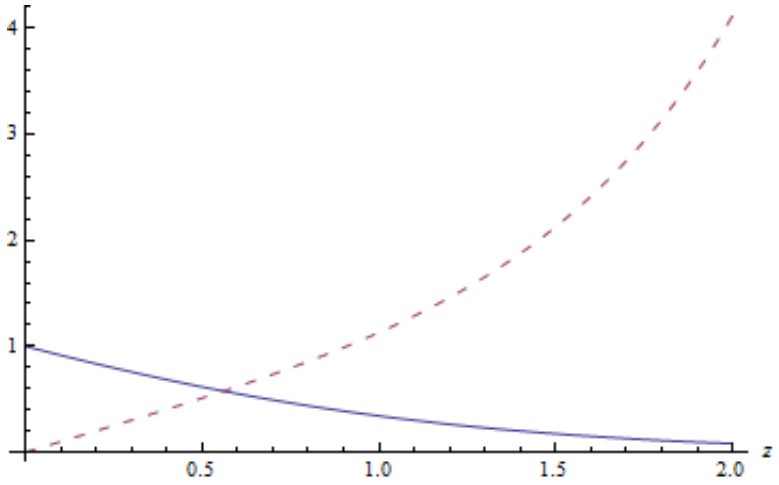

Fig. II.1. : $F(z)$ (solid) and $G(z)$ (dashed) for $\alpha = 1$, $\kappa = .5$

For $\alpha = 2$, the solutions are

$$F(z) = \frac{\mathrm{D}_{-(\kappa^2+1)/2}(\sqrt{2}z)}{\mathrm{D}_{-(\kappa^2+1)/2}(0)} \tag{II.7}$$

$$G(z) = \frac{\mathrm{D}_{-(\kappa^2+1)/2}(-\sqrt{2}z) - \mathrm{D}_{-(\kappa^2+1)/2}(\sqrt{2}z)}{2\sqrt{2}\,\mathrm{D}_{-(\kappa^2+1)/2}(0)}. \tag{II.8}$$

Unfortunately, there are no known closed-form solutions to the differential equation when $\alpha > 2$.

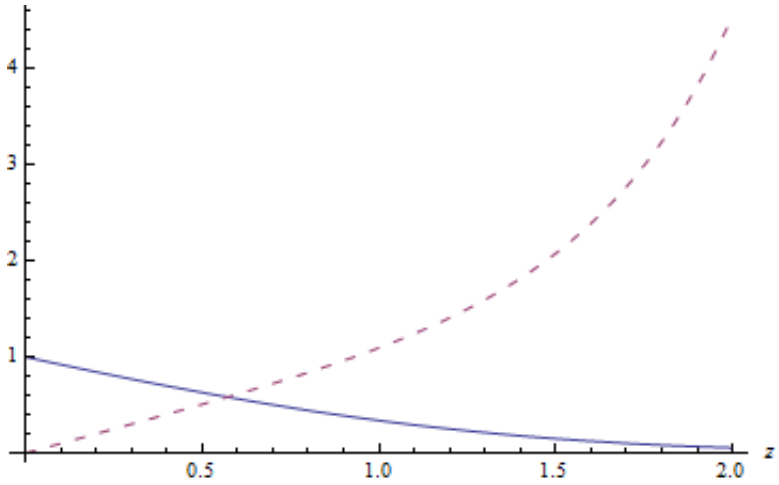

Fig. II.2. : $F(z)$ (solid) and $G(z)$ (dashed) for $\alpha = 2$, $\kappa = .5$

Since we intend to examine the limiting case as $\alpha \to \infty$, we will need to find numerical solutions to these equations. Direct computation of the solutions via numerical methods is time-consuming and inefficient except for very small values of α. As such, our next step is to find more general methods of characterizing these solutions.

The two approximations we use come from WKB and perturbation calculations. The WKB solution arises from approximating the solution to the differential equation as a product of exponential terms. The solutions can be approximated by

$$F(z) \approx c_F(\kappa^2 + z^\alpha)^{-\frac{1}{4}} \exp\left[-\int dz \left(\sqrt{\kappa^2 + z^\alpha} + \frac{V''}{8(\kappa^2 + z^\alpha)^{\frac{3}{2}}}\right)\right] \tag{II.9}$$

$$G(z) \approx c_G(\kappa^2 + z^\alpha)^{-\frac{1}{4}} \sinh\left[\int dz \left(\sqrt{\kappa^2 + z^\alpha} + \frac{V''}{8(\kappa^2 + z^\alpha)^{\frac{3}{2}}}\right)\right] \tag{II.10}$$

where c_F and c_G are constants used to match the normalization conditions [14].

The perturbation calculations were begun by J. Wagner [15] using eigenfunctions. In this technique, we can write the exact solution in an infinite series in κ^2. In the region near $\kappa = 0$, the solution can be approximated by a term constant in κ plus a term proportional to κ^2:

$$F(z) \approx F_0(z) + \kappa^2 F_1(z) \tag{II.11}$$

$$G(z) \approx G_0(z) + \kappa^2 G_1(z) \tag{II.12}$$

The separated field equation can be solved exactly when $\kappa = 0$. Using the notation

$$\beta = \frac{1}{\alpha + 2} \tag{II.13}$$

$$k(z) = \sqrt{z} K_\beta\left(2\beta z^{\frac{1}{2\beta}}\right) \tag{II.14}$$

$$i(z) = \sqrt{z} I_\beta\left(2\beta z^{\frac{1}{2\beta}}\right) \tag{II.15}$$

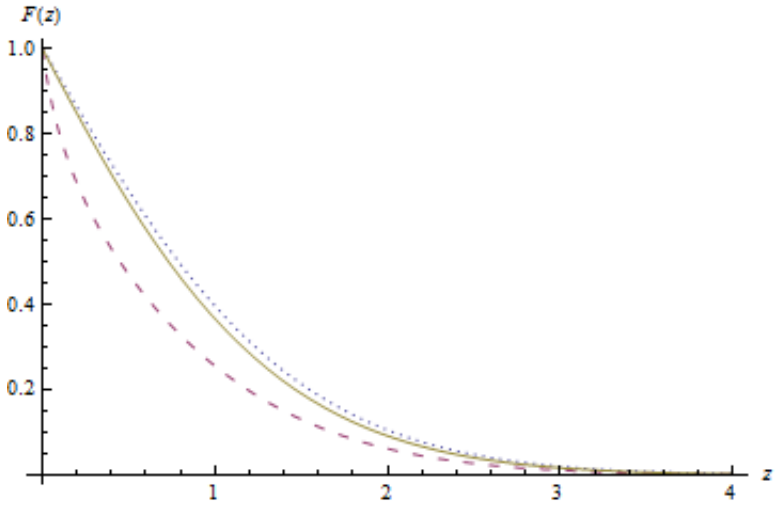

Fig. II.3. Exact (solid), WKB (dashed), and perturbation (dotted) solutions of F(z) for $\alpha = 1$, $\kappa = 0.3$. The perturbation solution closely matches the exact solution.

where K and I represent the Bessel K and Bessel I functions, respectively, we can then write

$$F_0(z) = c_1 k(z) \tag{II.16}$$

$$G_0(z) = c_2 i(z) \tag{II.17}$$

and

$$F_1(z) = \frac{1}{W(i,k)} \left(k(z) \int_0^z i(a) F_0(a) da + i(z) \int_z^\infty k(a) F_0(a) da \right) \tag{II.18}$$

$$G_1(z) = \frac{1}{W(i,k)} \left(i(z) \int_0^z k(a) G_0(a) da - k(z) \int_0^z i(a) G_0(a) da \right) \tag{II.19}$$

where c_1 and c_2 are constants used to match the normalization conditions, and $W(i,k)$ is the Wronskian of $i(z)$ and $k(z)$. We omit the derivations of Eq. II.18 and Eq. II.19, as they are analogous to those in [15]. In general, the WKB solutions are accurate when either κ or z are relatively large, and the perturbation solutions are more accurate when κ and z are small.

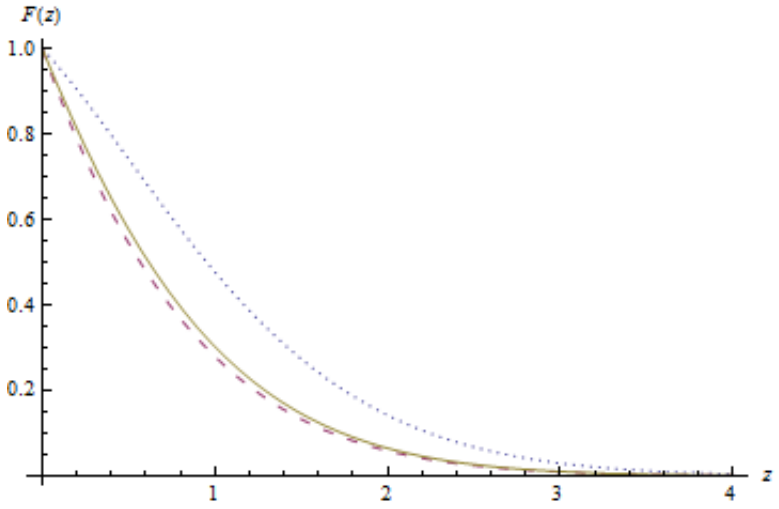

Fig. II.4. Exact (solid), WKB (dashed), and perturbation (dotted) solutions of F(z) for $\alpha = 1$, $\kappa = 0.75$. The WKB solution closely matches the exact solution.

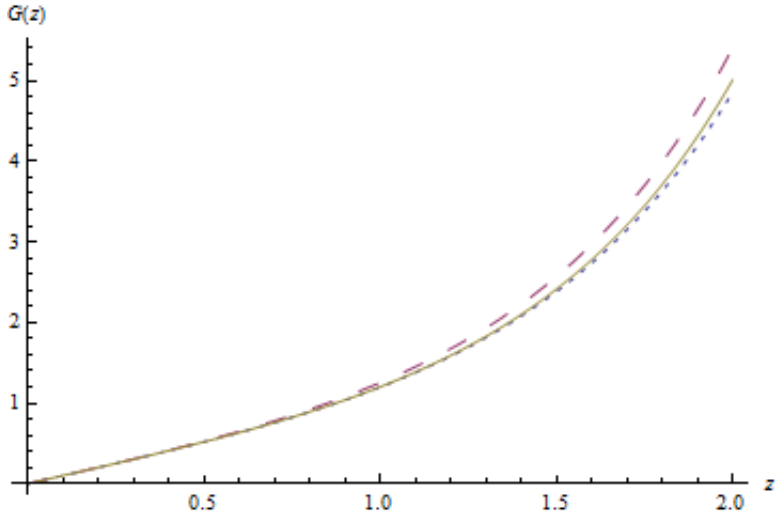

Fig. II.5. Exact (solid), WKB (large dashed), and perturbation (small dashed) solutions of G(z) for $\alpha = 1$, $\kappa = 0.8$. The perturbation solution closely matches the exact solution.

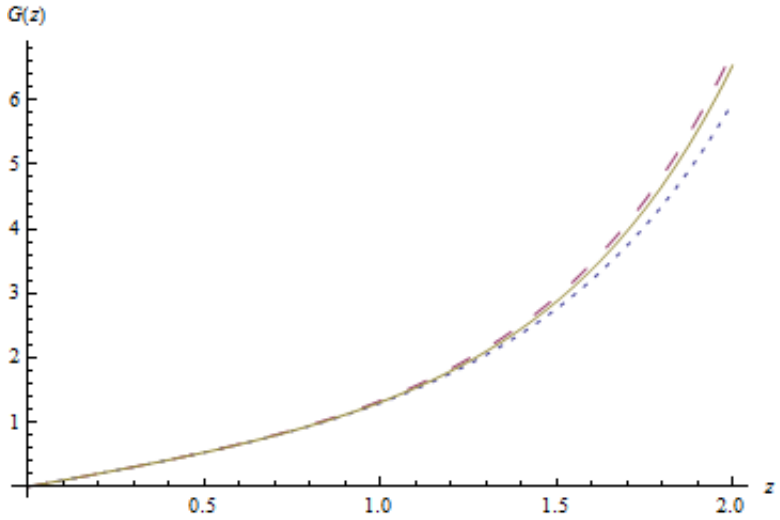

Fig. II.6. Exact (solid), WKB (large dashed), and perturbation (small dashed) solutions of G(z) for $\alpha = 1$, $\kappa = 1.1$ The WKB solution closely matches the exact solution.

Stress-Energy Tensor

We begin with the general definition of the stress-energy tensor acting on a massless scalar field [16] with conformal parameter ξ and mode function Φ,

$$\begin{aligned} T_{\mu\nu} =& \partial_\mu \Phi \partial_\nu \Phi - \frac{1}{2} g_{\mu\nu} (\partial_\lambda \Phi \partial^\lambda \Phi + V \Phi^2) \\ &+ \xi (\partial_\mu \partial_\nu - g_{\mu\nu} \partial_\lambda \partial^\lambda) \Phi^2. \end{aligned} \tag{II.20}$$

We then declare that $g_{\mu\nu}$ is the Lorentz space-time tensor $\eta_{\mu\nu} = \text{diag}(-1, 1, 1, 1)$.

It is readily shown that the off-diagonal terms of $T_{\mu\nu}$ vanish for a single conducting plane. Furthermore, it is possible to induce the equation of motion (as done in [16]) $(\Box + V)\Phi = 0$ to simplify our expressions for $T_{\mu\nu}$. Therefore, the most mathematically convenient forms of the energy density and pressure are

$$T_{00} = \frac{1}{2}(\partial_0 \Phi)^2 - \frac{1}{2}\Phi(\partial_0)^2 \Phi - \beta \nabla^2 \Phi^2 \tag{II.21a}$$

$$T_{11} = \frac{1}{2}(\partial_1 \Phi)^2 - \frac{1}{2}\Phi(\partial_1)^2 \Phi + \beta(-\partial_0^2 + \partial_2^2 + \partial_3^2)\Phi^2, \tag{II.21b}$$

where $\beta = \xi - \frac{1}{4}$ was chosen for notational convenience. The terms T_{22} and T_{33} can be found by interchanging the indices 1 and 2 or 3 respectively in T_{11}.

It is possible to take a Fourier transform of the stress-tensor elements to get relations that do not explicitly depend on the field Φ, instead writing them in terms of the Green's function $g_\kappa(z, z')$. We begin with the definition of the Fourier transform of the vacuum expectation value of a tensor component,

$$\langle T_{\mu\nu} \rangle = \int \frac{d\zeta}{2\pi} \frac{d\boldsymbol{k}_\perp}{(2\pi)^2} e^{-i\omega(t-t')} e^{i\boldsymbol{k}_\perp \cdot (r-r')_\perp} t_{\mu\nu} \Big|_{z' \to z} \tag{II.22}$$

$$= \int \frac{d\zeta}{2\pi} \frac{d\boldsymbol{k}_\perp}{(2\pi)^2} e^{i\zeta\tau} e^{i\boldsymbol{k}_\perp \cdot \boldsymbol{r}_\perp} t_{\mu\nu} \Big|_{z' \to z}, \tag{II.23}$$

where $t_{\mu\nu}$ is the Fourier transformed tensor component. Here we have taken the Euclidean rotation

$$\omega \to i\zeta, \qquad (t - t') \to i\tau \tag{II.24}$$

and made the variable substitution

$$(r - r')_\perp = \boldsymbol{r}_\perp \tag{II.25}$$

following the work of Milton [14]. The four-vector $\boldsymbol{r} = (\tau, \boldsymbol{r}_\perp, (z - z'))^\intercal$ is the point-splitting vector that regularizes our expression for the vacuum energy and pressure.

To find $t^{\mu\nu}$, we begin with the relation

$$\langle 0|\Phi(z)\Phi(z')|0\rangle = \frac{1}{i}G(z, z') \tag{II.26}$$

$$G(z, z') = \int \frac{d\zeta}{2\pi}\frac{d\boldsymbol{k}_\perp}{(2\pi)^2}e^{i\zeta\tau}e^{i\boldsymbol{k}_\perp\cdot\boldsymbol{r}_\perp}g_\kappa(z, z'), \tag{II.27}$$

where $G(z, z')$ is the inverse Fourier transform of the Green's function as defined earlier in the paper. Let $g_\kappa(z, z)$ represent the Green's function after z' has been set to z. Taking the Fourier transform of $T_{\mu\nu}$, we find the stress-energy tensor components to be

$$t_{00} = -\zeta^2 g_\kappa(z, z) - 2\beta(\partial_z^2 + \partial_z\partial'_z)g_\kappa(z, z')\big|_{z'\to z} \tag{II.28a}$$

$$t_{11} = k_1^2 g_\kappa(z, z) + 2\beta(\partial_z^2 + \partial_z\partial'_z)g_\kappa(z, z')\big|_{z'\to z} \tag{II.28b}$$

$$t_{22} = k_2^2 g_\kappa(z, z) + 2\beta(\partial_z^2 + \partial_z\partial'_z)g_\kappa(z, z')\big|_{z'\to z} \tag{II.28c}$$

$$t_{33} = \frac{1}{2}(\partial_z^2 - \partial_z\partial'_z)g_\kappa(z, z')\big|_{z'\to z}. \tag{II.28d}$$

Putting these together with Eq. II.22 and Eq. II.23, we obtain a formula for T_{00} and similar formulas for the other components. Specifically,

$$\begin{aligned}\langle T_{00}\rangle = \int \frac{d\zeta}{2\pi}\frac{d\boldsymbol{k}_\perp}{(2\pi)^2}e^{i\zeta\tau}e^{i\boldsymbol{k}_\perp\cdot\boldsymbol{r}_\perp} \\ \times [-\zeta^2 g_\kappa(z, z) - 2\beta(\partial_z^2 + \partial_z\partial'_z)g_\kappa(z, z')\big|_{z'\to z}].\end{aligned} \tag{II.29}$$

Following the work of Milton [14], let us make a change of variable to polar coordinates. We define the polar variables

$$\kappa^2 = |\boldsymbol{k}_\perp|^2 + \zeta^2 \qquad \cos\theta = \frac{\zeta}{\kappa}$$
$$\delta^2 = |\boldsymbol{r}_\perp|^2 + \tau^2 \qquad \cos\phi = \frac{k_1}{|\boldsymbol{k}_\perp|}$$

and make use of the total derivative

$$\frac{d^2}{dz^2}\Big[g_\kappa(z,z')\big|_{z'\to z}\Big] = 2\Big[\frac{\partial^2}{\partial z^2}g_\kappa(z,z')\big|_{z'\to z} + \frac{\partial}{\partial z}\frac{\partial}{\partial z'}g_\kappa(z,z')\big|_{z'\to z}\Big] \tag{II.30}$$

to rewrite the z and z' derivatives of g_κ in equation II.28 as a total derivative of g_κ, after z' has been set to z. We then rewrite this equation as

$$\langle T_{00}\rangle = \frac{1}{(2\pi)^3}\left(\frac{\partial^2}{\partial\tau^2} - \beta\frac{\partial^2}{\partial z^2}\right)\int_0^\infty d\kappa\kappa\int_{-1}^1 d\cos\theta \times \int_0^{2\pi} d\phi e^{i\kappa\sin\theta(\cos\phi r_1+\sin\phi r_2)}e^{i\kappa\cos\theta\tau}g_\kappa(z,z) \tag{II.31}$$

and integrate over the angular coordinates. Doing the same for the other components, we finally arrive at the expectation values of the stress-energy tensor components:

$$\langle T_{00}\rangle = \frac{1}{2\pi^2}\left(\frac{\partial^2}{\partial\tau^2} - \beta\frac{\partial^2}{\partial z^2}\right)\int_0^\infty d\kappa\kappa g_\kappa(z,z)\frac{\sin\kappa\delta}{\delta} \tag{II.32a}$$

$$\langle T_{11}\rangle = \frac{1}{2\pi^2}\left(-\frac{\partial^2}{\partial r_1^2} + \beta\frac{\partial^2}{\partial z^2}\right)\int_0^\infty d\kappa\kappa g_\kappa(z,z)\frac{\sin\kappa\delta}{\delta} \tag{II.32b}$$

$$\langle T_{22}\rangle = \frac{1}{2\pi^2}\left(-\frac{\partial^2}{\partial r_2^2} + \beta\frac{\partial^2}{\partial z^2}\right)\int_0^\infty d\kappa\kappa g_\kappa(z,z)\frac{\sin\kappa\delta}{\delta} \tag{II.32c}$$

$$\langle T_{33}\rangle = \frac{1}{2\pi^2}\int_0^\infty d\kappa\kappa\left[\left(\frac{\partial^2}{\partial z^2} - \frac{\partial}{\partial z}\frac{\partial}{\partial z'}\right)g_\kappa(z,z')\right]\Bigg|_{z'\to z} \times\frac{\sin\kappa\delta}{\delta}. \tag{II.32d}$$

It is readily seen that the only dependence remaining on the point splitting variable inside the integral is in the scalar delta. To find the formal (infinite) energy density and pressure, let $\delta \to 0$. From this form of the stress-energy tensor, it can readily be shown that the pressure anomaly is resolved. We first look at the transverse pressures. In the limit $\delta \to 0$, $T_{00} = -T_{11} = -T_{22}$, so we have recovered the expected relation between energy density and pressure as predicted by the principle of virtual work. To visualize this, place a test wall perpendicular to the existing soft wall. If a pressure on this wall pushes the test wall, there will be a decrease in energy corresponding to the amount of work done in the process of moving the test wall. Finally, we consider the perpendicular pressure T_{33}. In the limit $\delta \to 0$, the integrand of T_{33} becomes identically zero for all values of κ, so $T_{33} = 0$. However, this is not a violation of the principle of virtual work, because the configuration of the system has not changed. If the soft wall were to move in the z-direction, it would be akin to a change in the origin of the coordinate system, and therefore no work is done on the vacuum energy.

CHAPTER III

OUTSIDE THE WALL

Given the expressions for F and G computed in Chapter II, we can define the Green's function outside the wall. [14] Defining

$$\gamma_-(\kappa) = \frac{\kappa + F'(0)}{\kappa - F'(0)}, \tag{III.1}$$

we compute the Green's function to be

$$g(z, z') = \frac{1}{2\kappa} e^{-\kappa|z-z'|} + \frac{1}{2\kappa} e^{\kappa(z+z')} \gamma_-(\kappa). \tag{III.2}$$

The first term is the vacuum term, which exists even in the absence of the wall. This term has been exhaustively studied already; more can be read about it in almost any introductory text to the Casimir effect (for example, [17]). The second term is used to find the effect of the wall on space outside the wall.

The next step is to compute the energy density. This can be derived from the Green's function [14], giving a result of

$$u(z) = \frac{1 - 6\xi}{6\pi^2} \int_0^\infty d\kappa \kappa^3 e^{2\kappa z} \gamma_-(\kappa), \tag{III.3}$$

where ξ is the conformal parameter. Using the form given by Milton [14] for $F(\kappa)$ in the limit as $\kappa \to \infty$, we arrive at

$$\gamma_-(\kappa) \approx -\frac{\Gamma(\alpha + 1)}{(2\kappa)^{\alpha+2}}. \tag{III.4}$$

Similarly, we can use the perturbative form of $F(\kappa)$ for small κ to get

$$\gamma_-(\kappa) \approx \frac{\kappa + F_0'(0) + \kappa^2 F_1'(0)}{\kappa - F_0'(0) - \kappa^2 F_1'(0)} \tag{III.5}$$

These two approximations match the form of $\gamma_-(\kappa)$ very well for large and small κ, respectively, but there is a significant intermediate region in which neither is accurate. We remedy this by introducing a spline function

$$s(\kappa) = e^{a+b\kappa}, \tag{III.6}$$

where a and b are values chosen such that

$$s(d_1) = -\left(1 + \frac{2d_1}{F_0'(d_1)} + \frac{2d_1^2}{(F_0'(d_1))^2}\right) \tag{III.7}$$

$$s(d_2) = -\frac{\Gamma(\alpha+1)}{(2d_2)^{\alpha+2}} \tag{III.8}$$

for some arbitrary values d_1 and d_2. That is, the spline is an exponential function that connects a point d_1 on the perturbation solution to a point d_2 on the large-κ solution. The accuracy of this spline compared to the actual solution depends on the choices for the points d_1 and d_2. When the exact form of the solution is known, one can simply adjust the parameters as needed until the spline is optimized; however, this cannot be performed for $\alpha > 2$ because there are no closed-form solutions. To arrive at a suitable set of boundary points without knowing the form of the exact solution, we use Newton's Method to match the derivative of the spline function to the derivatives of the approximations at the points of intersection. In addition to providing a reasonable estimate of the exact solution, this derivative-matched spline also ensures the smoothness of our approximation for $\gamma_-(\kappa)$. Some plots of these approximations are given on the next page. Now that we have the form of $\gamma_-(\kappa)$, we can use this to find the energy density outside the wall. After finding the optimum values for d_1 and d_2 for a given value of α, we approximate $\gamma_-(\kappa)$ with a piecewise function given by the perturbation solution when $\kappa < d_1$, the spline function when $d_1 < \kappa < d_2$, and the large-κ solution when $d_2 < \kappa$.

It is possible to show qualitatively that our approximation is an upper bound. From the form of the differential equation for ϕ, it is readily seen that $\phi_\kappa''(z)$ is monotonically decreasing over the range $z > 0$. Therefore, the perturbation expansion, which matches the value of the function and its first two derivatives, is strictly larger than the exact solution.

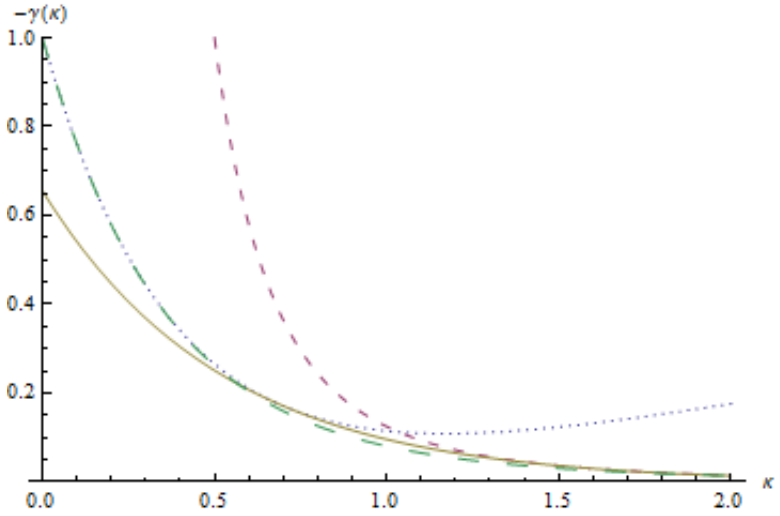

Fig. III.1. : Approximations (perturbation in dots, large-κ in small dashes, spline in solid line) and exact solution (large dashes) for the $\alpha = 1$ case.

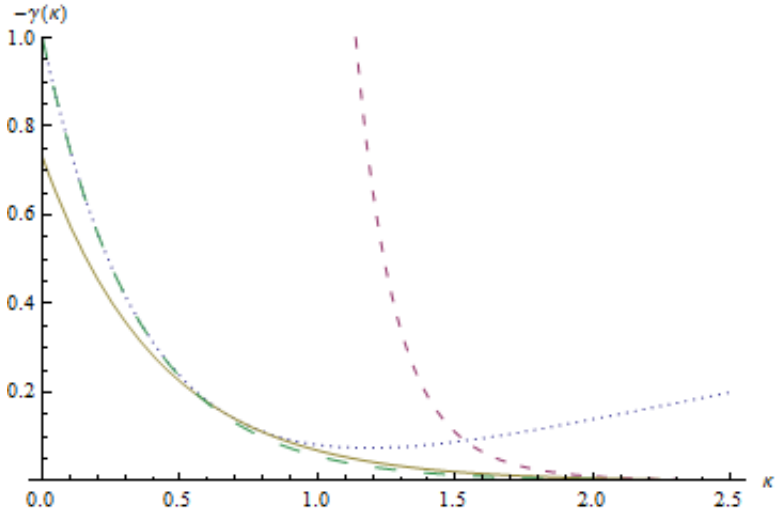

Fig. III.2. : Approximations (perturbation in dots, large-κ in small dashes, spline in solid line) for the $\alpha = 6$ case. A numerical approximation of the exact solution, computed using Mathematica, is shown in large dashes. Notice that the spline continues to match the exact function even when the two series approximations are far apart.

The WKB expansion and the spline approximation forms of γ_- are strictly larger than the exact solution in the special cases where it can be calculated. Furthermore, they appear to follow the same relation with the numerical solutions to the equation. As such, we believe that our methods give an over-approximation of the solution.

It is also worth noting that due to the form of the large-κ solution, $u(0)$ will converge only for $\alpha > 2$. Finally, we compare our value of $u(0)$ as a function of α to the value computed by Milton.

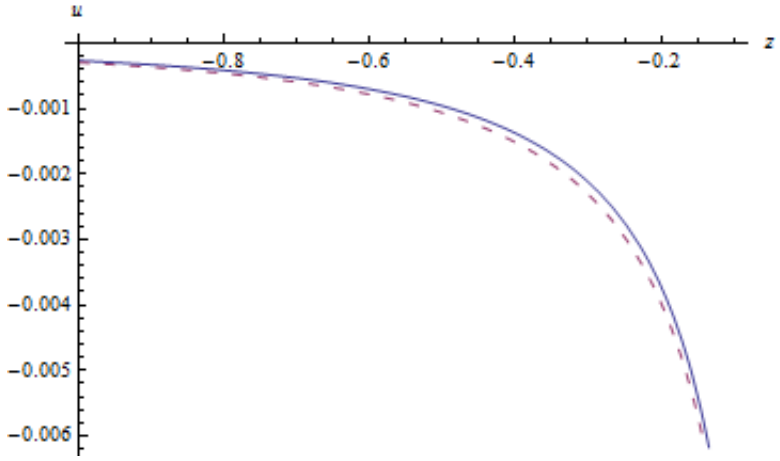

Fig. III.3. : Approximation (dashed) and exact solution (solid) for T_{00} outside the wall in the $\alpha = 1$ case. The factor of $1 - 6\xi$ is omitted.

[14] The new method creates a much more suitable upper bound because it diverges much more slowly as α increases.

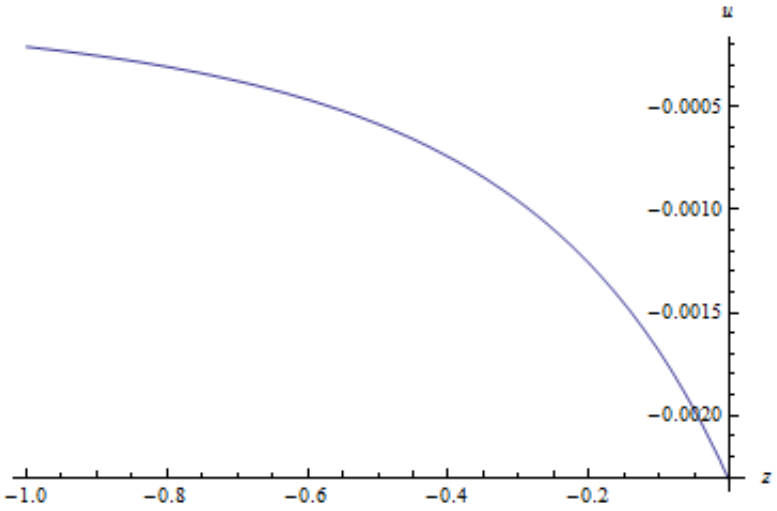

Fig. III.4. : Approximation for T_{00} outside the wall in the $\alpha = 6$ case. The factor of $1 - 6\xi$ is omitted.

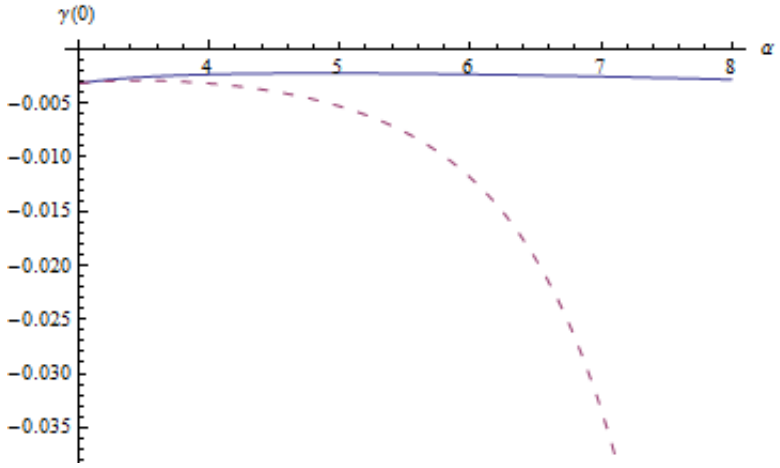

Fig. III.5. Our approximation (solid) and Milton's approximation (dashed) for $u(0)$ as a function of α. The factor $1 - 6\xi$ is omitted.

CHAPTER IV

INSIDE THE WALL

The problem of finding energy density inside the wall, where the potential is nonzero, is substantially more difficult than the case outside the wall. We begin, as we did before, by finding the Green's function [18], given by

$$g_\kappa(z, z') = (G(z) + \gamma_+ F(z))\, F(z) \tag{IV.1}$$

where we have introduced the function

$$\gamma_+ = \frac{1}{\kappa - F'(0)} \tag{IV.2}$$

Once again, we would like to find approximations for this quantity in order to facilitate computation of the energy density. We can use the WKB form of $F(z)$ in the high κ region to find

$$\gamma_+(\kappa) \approx \frac{1}{2\kappa} \tag{IV.3}$$

In the region of small κ, we can approximate $F'(0) \approx F_0'(0)$ and get

$$\gamma_+(\kappa) \approx \frac{1}{\kappa + \beta^{2\beta-1}\Gamma(1-\beta)/\Gamma(\beta)} \tag{IV.4}$$

where

$$\beta = \frac{1}{\alpha + 2}. \tag{IV.5}$$

By using the perturbative form of $\gamma_+(\kappa)$ as well as the perturbation solutions for $F(z)$ and $G(z)$ computed in Eq. II.11 and Eq. II.12, we can find a reasonable approximation for the Green's function in the region where κ is small. Similarly, the WKB form of $\gamma_+(\kappa)$ and the WKB solutions for $F(z)$ and $G(z)$ constitute the asymptotic behavior of the Green's function in the region where

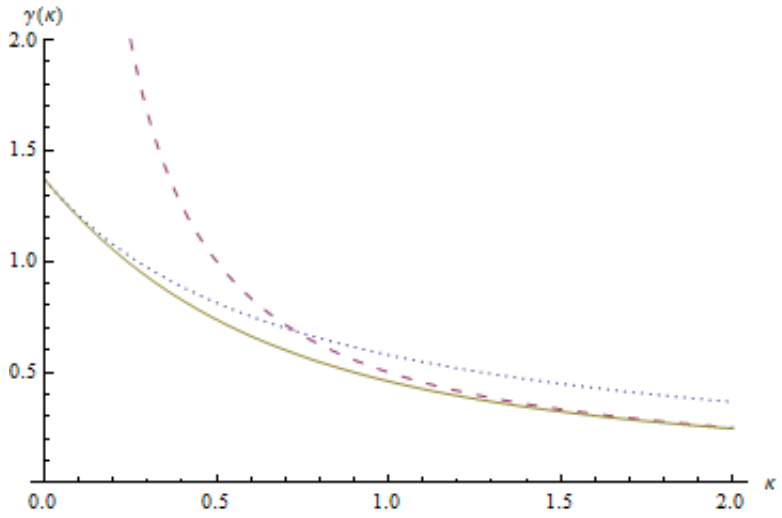

Fig. IV.1. : $\gamma^{+}(\kappa)$. The solid line is the exact solution, the dotted line is the perturbation expansion, and the dashed line is the WKB approximation.

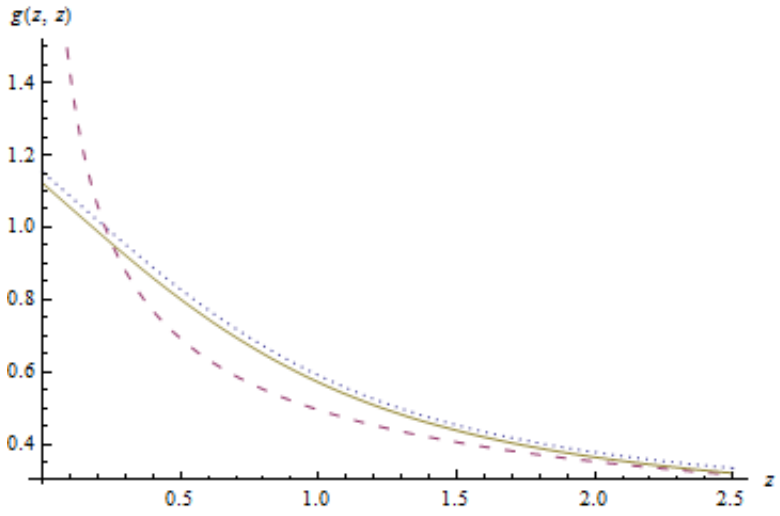

Fig. IV.2. : $g_\kappa(z,z)$ for $\kappa = 0.15$. The solid line is the exact solution, the dotted line is the perturbation expansion, and the dashed line is the WKB approximation. The perturbation expansion is quite good here throughout our range of z, whereas the WKB expansion takes a long time to converge to the correct value.

κ is large. In order to find a consistently reasonable approximation for the Green's function, we would need a spline function to connect the two regimes; however, the process is more difficult than it was outside the wall. In this case, the approximations inside the wall must hold up for all possible values of z, as the Green's function depends on this value as well as on κ. The energy density inside the wall is dependent upon the Green's function [14]. In this region,

$$u = \frac{1}{8\pi^2}\left[(1-4\xi)\frac{\partial^2[}{\partial,^2}z] + 4\frac{\partial^2[}{\partial,^2}\tau]\right]\int_0^\infty d\kappa\kappa g(z,z)\frac{\sin\kappa\tau}{\tau} \tag{IV.6}$$

Due to the difficulty of working with the Green's function inside the wall, we do not yet have a working spline approximation in that region. Furthermore, we would still like to expand on Milton's work inside the wall by carrying out the Weyl expansion of the energy density (equation 4.20 in [14]) using the 3rd order WKB approximation. By doing so, we hope to recover the physical, finite terms of the energy density and pressure, from which point we could determine whether the pressure anomaly is resolved inside the wall.

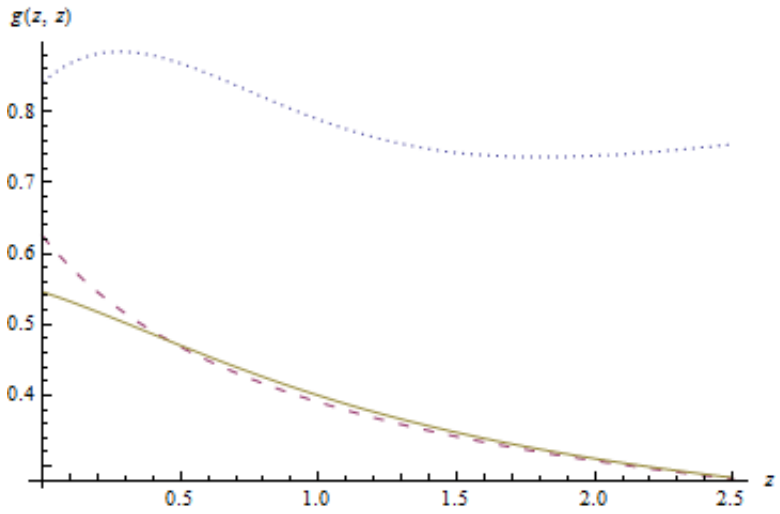

Fig. IV.3. : $g_\kappa(z,z)$ for $\kappa = 0.8$. The solid line is the exact solution, the dotted line is the perturbation expansion, and the dashed line is the WKB approximation. The perturbation expansion is poor here, but the WKB expansion quickly converges to a reasonable value.

The third order terms of the WKB expansion can be derived using the approach provided by Fröman. Using the algebraic manipulations performed in [19], it is possible to rewrite the WKB series in such a way that each of the terms in the phase integral is also present in the amplitude, preserving the Wronskian of the original differential equation. The third order WKB series of F and G under this scheme are given by

$$F(z) = \frac{C_F}{\sqrt{Q_\kappa(z) + \frac{V''(z)}{8Q_\kappa(z)^3}}} e^{-\int^z dz Q_\kappa(z) + \frac{V''(z)}{8Q_\kappa(z)^3}} \tag{IV.7}$$

$$G(z) = \frac{C_G}{\sqrt{Q_\kappa(z) + \frac{V''(z)}{8Q_\kappa(z)^3}}} \sinh\left(\int^z dz Q_\kappa(z) + \frac{V''(z)}{8Q_\kappa(z)^3}\right) \tag{IV.8}$$

where

$$V(z) = z^\alpha \tag{IV.9}$$

$$Q_\kappa(z) = \sqrt{\kappa^2 + z^\alpha}. \tag{IV.10}$$

The integral in the WKB approximation is exactly evaluable for all positive $\alpha > 2$, and the special cases $\alpha = 1$ and $\alpha = 2$. Denoting this integral as $I_{\kappa,\alpha}(z)$, in the special cases, it evaluates to the following:

$$I_{\kappa,\alpha}(z) = \begin{cases} \frac{2}{3}(Q^3 - \kappa^3) + \frac{1}{8\kappa^3} & \text{if} \quad \alpha = 1 \\ \frac{z + 2z^3\kappa^2 + 2z\kappa^4 + 2\kappa^4 Q \sinh^{-1}\left(\frac{z}{\kappa}\right)}{4\kappa^2 Q} & \text{if} \quad \alpha = 2. \end{cases} \tag{IV.11}$$

For the general $\alpha > 2$ case, it evaluates to the following:

$$\begin{aligned} I_{\kappa,\alpha}(z) = \frac{1}{8z\kappa^3 Q^2} \Bigg[& 8z^2\kappa^4 Q^2 {}_2F_1\left(-\frac{1}{2}, \frac{1}{\alpha}; 1 + \frac{1}{\alpha}; -\frac{V(z)}{\kappa^2}\right) \\ & + V(z)(-2 + 3\alpha)\kappa^2 {}_2F_1\left(-\frac{1}{2}, \frac{\alpha - 1}{\alpha}; 2 - \frac{1}{\alpha}; -\frac{V(z)}{\kappa^2}\right) \\ & - V(z)(V(z)(\alpha - 2) + 2(\alpha - 1)\kappa^2) {}_2F_1\left(\frac{1}{2}, \frac{\alpha - 1}{\alpha}; 2 - \frac{1}{\alpha}; -\frac{V(z)}{\kappa^2}\right) \Bigg]. \end{aligned} \tag{IV.12}$$

To actually apply this form of the WKB series, we would first take an asymptotic expansion of the exact integrals, and plug them into the green's function as done in section 4 of [14]. We then evaluate the energy density integral, and look for terms that remain finite and non-zero as the point-splitting vector δ goes to zero. In particular, if the finite terms of the energy density converge to the same value regardless of the order in which the point splitting components (τ and $\boldsymbol{r}$) are removed, then the pressure anomaly is resolved for the parallel directions. We hope to carry out the calculation outlined above in the future.

CHAPTER V

CONCLUSIONS

The soft-wall model has proven to be a powerful tool for examining the Casimir effect on a single boundary. We have defined the soft-wall model and described the solutions to the separated field equation along with some useful approximations. We have also found the components of the stress-energy tensor and shown that the pressure anomaly is resolved outside the wall. In the region outside the wall, we have shown approximations for energy density that closely match the exact solutions for wide range of α. Finally, we have provided approximations for the Green's function and energy density in the region of nonzero potential. We hope that this will act as a groundwork from which it will be possible to resolve the pressure anomaly inside the wall. In conclusion, we hope that our work on the soft-wall model will allow a much broader range of Casimir systems to be effectively studied, broadening our understanding of one of the most enigmatic fields of current physics research.

REFERENCES

[1] D. Dalvit, P. Milonni, D. Roberts, and F. da Rosa, *Casimir Physics*, no. 834 in Lecture Notes in Physics, Springer2011.

[2] K. A. Milton, *The Casimir Effect: Physical Manifestations of Zero-Point Energy*, World Scientific2001.

[3] H. B. G. Casimir, *On the Attraction Between Two Perfectly Conducting Plates*, Proc. Kon. Nederland Akad. Wetensch. **B51** (1948) 793–795.

[4] D. Deutsch and P. Candelas, *Boundary Effects in Quantum Field Theory*, Phys. Rev. D **20** (1979) 3063.

[5] S. A. Fulling, C. S. Trendafilova, P. N. Truong, and J. Wagner, *Wedges, Cones, Cosmic Strings, and the Reality of Vacuum Energy*, Int. J. Mod. Phys. A **45** (2012) 374018.

[6] S. A. Fulling, F. D. Mera, and C. S. Trendafilova, *Torque Anomaly in Quantum Field Theory*, Phys. Rev. D **87** (2013) 047702.

[7] T. H. Boyer, *Quantum Electromagnetic Zero-Point Energy of a Conducting Spherical Shell and the Casimir Model for a Charged Particle*, Phys. Rev. **174** (1968) 1764.

[8] S. A. Fulling, *Vacuum Energy Density and Pressure Near Boundaries*, Int. J. Mod. Phys. A **25** (2010) 2367–2372.

[9] S. A. Fulling, L. Kaplan, K. Kirsten, Z. H. Liu, and K. A. Milton, *Rectangles, Pistons, and Pistols*, J. Phys. A **42** (2009) 155402.

[10] R. Estrada, S. A. Fulling, and F. D. Mera, *Surface Vacuum Energy in Cutoff Models: Pressure Anomaly and Distributional Gravitational Limit*, J. Phys. A **45** (2012) 455402.

[11] J. P. Dowling, *The Mathematics of the Casimir Effect*, Math. Mag. **62** (1989) 5 324–331.

[12] S. A. Fulling, K. A. Milton, and J. Wagner, *Energy Density and Pressure in Power-Wall Models*, Int. J. Mod. Phys. A **27** (2012) 1260009.

[13] J. D. Bouas, S. A. Fulling, F. D. Mera, K. Thapa, C. S. Trendafilova, and J. Wagner, *Investigating the Spectral Geometry of a Soft Wall*, in A. H. B. et al., ed., *Spectral Geometry*, vol. 84, AMS, Providence2011.

[14] K. A. Milton, *Hard and Soft Walls*, Phys. Rev. D **84** (2011) 065028.

[15] J. Wagner, *Power Wall* (2010), ed. by S. A. Fulling and F. Mera (unpublished).

[16] K. A. Milton, K. V. Shajesh, S. A. Fulling, and P. Parashar, *How Does Casimir Energy fall? IV. Gravitational Interaction of Regularized Quantum Vacuum Energy*, Phys. Rev. D **88** (2014) 064027.

[17] G. Plunien, B. Müller, and W. Greiner, *The Casimir Effect*, Physics Reports **134** (1986) 2 - 3 87 – 193.

[18] J. Wagner, L. Kaplan, F. Mera, and S. A. Fulling, *The Perturbation Series for the Power Wall* (2010), (unpublished).

[19] N. Fröman, Ark. Fys. **32** (1966) 541.